Composites: Part A 101 (2017) 408–421

Contents lists available at ScienceDirect

Composites: Part A

journal homepage: www.elsevier.com/locate/compositesa

Heater power control for multi-material, variable speed Automated Fibre Placement

Mattia Di Francesco [a,*], Laura Veldenz [a], Giuseppe Dell'Anno [a], Kevin Potter [b]

[a] The National Composites Centre, Bristol and Bath Science Park, Bristol BS16 7FS, UK
[b] Advanced Composites Centre for Innovation and Science, Department of Aerospace Engineering, University of Bristol, Bristol BS8 1TR, UK

ARTICLE INFO

Article history:
Received 31 January 2017
Received in revised form 23 May 2017
Accepted 13 June 2017
Available online 19 June 2017

Keywords:
A. Polymer-matrix composites (PMCs)
B. Thermal properties
C. Process modelling
D. Automated fibre placement (AFP)

ABSTRACT

Automated Fibre Placement requires accurate control of the heater power to deposit the material at appropriate temperatures throughout the process. This paper presents a simple semi-empirical thermal model of the process which correlates the heater power and the layup speed with the substrate surface temperature. The deposition temperature was measured over a range of heater powers and layup speeds. The experimental data is used to define and validate a semi-empirical thermal model for two classes of materials used in conjunction with a diode laser: carbon fibre reinforced thermoplastics and bindered dry fibres. This enables open-loop, speed dependent heater power control, based on defining and programming the speed dependent heater power function in the machine controls.

1. Introduction

Automated Fibre Placement (AFP) is a form of additive manufacturing for high performance continuous fibre reinforced polymeric composite materials. AFP is considered a key enabler for the exploitation of advanced composite materials in the aerospace industry and in other sectors. Generally speaking, an AFP machine consists of an automated manipulator (robotic, gantry, etc.) with an attached deposition head capable of depositing multiple individual composite tapes at once (a course) onto a mould tool. In its simplest form, the deposition head includes a tape feed and cut mechanism, a compaction device (usually a roller) and a heater [1]. The time dependent temperature and pressure required to adhere and consolidate the incoming tapes to the substrate depend on the raw material and the preform quality criteria [2–4].

Conventionally, three classes of composite materials are used in conjunction with AFP: continuous carbon fibre reinforced thermosets (generally epoxies) and thermoplastics [1], as well as bindered continuous carbon fibres [5].

Heat is supplied during deposition to ensure adhesion of the tapes to the previous ply or tool surface. Aerospace grade carbon fibre/epoxy prepregs behave like pressure sensitive adhesives. The material is moderately tacky at room temperature and only require a moderate increase in temperature above ambient to promote sufficient tackiness. Deposition at 20–70 °C is typical [6,7]. Thermoplastic pre-impregnated tapes require temperatures up to, and often in excess of, the matrix melt temperature in order to achieve a partial or complete weld to the previously deposited ply [8,9]. The melt temperature varies greatly between materials and it is in the 130–200 °C range for low performance commodity thermoplastic resins such as Polypropylene (PP) and Polyamide (PA) and 280–350 °C for high performance semi-crystalline thermoplastics such as Polyphenylene Sulfide (PPS) and Polyether Ether Ketone (PEEK). Bindered dry fibre tapes require processing temperatures in excess of the binder activation temperature, typically between 180 °C and 350 °C [5,10].

Infrared heaters are the industry standard heating system for the deposition of thermoset materials [1]. Hot Gas Torches (HGT) have been used for the layup of thermoplastic materials for more than two decades [11], the system is inexpensive, but difficult to control [12]. One of the more recently developed heat sources is a near Infrared (λ = 0.9–1.1 μm) fibre-coupled diode laser heating [1]. Despite the lower temperatures involved in the process, it is common to deposit dry-fibres materials with the aid of a laser system, as conventional IR heating systems are likely to slow down the process due to their relatively low power output. A bespoke system developed by Coriolis Composites and incorporating a 3-lamp IR heating system was reported to enable dry fibre layup up to 0.8 m/s only [13].

Thermosetting materials can be laid up successfully over a comparatively large temperature range, therefore it is common industrial practice to set the deposition unit to lay up the material at constant heater power, regardless of layup speed. On the other

* Corresponding author.
E-mail address: mattia.difrancesco@nccuk.com (M. Di Francesco).

http://dx.doi.org/10.1016/j.compositesa.2017.06.015
1359-835X/

hand, the layup of thermoplastic and dry-fibre materials involves higher temperatures and a comparatively smaller operating window [3]. A way of continuously controlling the laser power to achieve a constant temperature is required for anything other than constant speed deposition. The fast response of lasers (≈ 1 ms [14]), as opposed to infrared heaters (≈ 1–2 s [15]), has allowed the development of closed-loop temperature control systems. A long-wave infrared (LWIR) (λ = 6–15 μm) thermal camera, or another non-contact temperature measurement device can be used to monitor the surface temperature of the substrate and/or the incoming tape(s) at a discrete location or over an area. Such information is used to adjust the laser power (and sometimes orientation) continuously to achieve the desired material temperature in the "visible" section of the process [16]. Nevertheless, some lack of robustness in the closed-loop temperature control system has been reported [9,16]. This is most likely due to the large local temperature variations which occur as the result of local anomalies, such as tape edges, exposed fibres, splices and local changes of the fibre volume fraction [16], and/or the response rate of the system.

A more robust heater control system is required to achieve constant surface temperature during variable speed layup. So far, industry has used mostly trial and error procedures to determine the required heater power. Nevertheless, if the heater power required to maintain the nip-point temperature constant across a range of deposition speeds was known, such a function could be programmed into the machine control system. This would allow open-loop heater power control at variable deposition speed.

Firstly this paper defines the heater power control function analytically. Secondly, it develops, presents, and validates a novel experimental procedure and data processing method to determine the coefficients of the control function empirically. Then this work evaluates the impact of the difference between the analytically determined coefficients and the empirically determined ones. Finally, a set of coefficients is determined using a semi-empirical approach, which simplifies the experimental procedure.

This will be demonstrated for the layup of thermoplastic pre-impregnated tapes and bindered dry fibre tapes using a diode laser as the heat source.

2. Analytical model definition

Different solutions to the thermal problem have been proposed. These included a wide range of numerical thermal models; 3D transient solutions [17], 2D transient [18] and steady solutions [19,20], as well as 1D transient [21] and steady state solutions [22,23]. These models are sometimes coupled with a radiative heat flow model of the IR emitter [6], a computational fluid dynamic model of the gas flow from the HGT [24], or a two dimensional [23,25] or three dimensional [20,26] optical model of the laser beam. An inter-ply contact resistance model is sometime included [27].

These numerical solutions are flexible and can account for any change in the set-up and the material, but they are computationally expensive, complex to set-up and rely heavily on accurate characterisation of the material thermal properties. Moreover, it is challenging to account for the material and process variability often encountered in real processes.

The general heat diffusion equation in Cartesian coordinates for a homogeneous anisotropic material is

$$\rho c_p \frac{\delta T}{\delta t} = \nabla(\mathbf{k} \cdot \nabla T), \tag{1}$$

where ρ is the density, c_p is the specific heat capacity, **k** is the vector of thermal conductivities, t is the time, and T is the temperature. This can be reduced to its one-dimensional form in the through thickness direction (z) to

$$\rho c_p \frac{\delta T}{\delta t} \approx k_z \frac{\delta^2 T}{\delta z^2}. \tag{2}$$

The problem domain is then divided into three sub-domains: the incoming tape and the upstream composite substrate which when solved provide the initial conditions for the third domain, the downstream consolidated composite. The boundary conditions for all domains are defined according to

$$q_z(t) = k_z \frac{\delta T}{\delta z} = \overbrace{-h_c(T - T_\infty)}^{convection} - \overbrace{\sigma(T^4 - T_\infty^4)}^{radiation} + \overbrace{q_s(t)}^{heatsource}, \tag{2}$$

where $q_z(t)$ is the heat flux in the through thickness direction as a function of time, h_c is the convective heat transfer coefficient, T_∞ is the far field temperature, ϵ is the emissivity of the surface, σ is the Boltzmann constant, and q_s is the heat flux from the heat source [28].

A practical method to generate input data to any control algorithm is a conventional infrared (IR) camera. An IR camera can measure the surface temperature of the upstream composite substrate in the vicinity of the process nip-point, which is at an angle of incidence lower than 90°, typically 65–75°. The temperature of the incoming tapes in the vicinity of the process nip-point cannot be measured reliably by an IR camera because the angle of incidence in the region of interest approaches 90°. In this work, the measured surface temperature of the upstream composite substrate is used to define the control parameters for an open-loop control system. If a practical and validated analytical or numerical solution of the thermal problem is defined, the work could be extended to include open-loop control of the incoming tapes' temperature.

Idealising the substrate as a semi-infinite solid, defined as an idealised body that has a single plane surface and extends to infinity in all directions, the surface temperature at any time t can be calculated according to

$$T_s(t) = T_0 + \frac{2q_s}{k}\sqrt{\frac{\alpha t}{\pi}}, \tag{3}$$

where q_s is the heat flux from the heat source, k is the thermal conductivity, t is the time, and α is the thermal diffusivity, defined as the thermal conductivity, divided by material density (ρ), and the specific heat capacity (c_p) [29]. This can be done on the basis of the following assumptions:

- the substrate has constant thermophysical properties,
- there is no internal heat generation,
- the substrate is exposed to a uniform heat flux on its exposed surface,
- there is no heat loss to the environment,
- the initial temperature (T_0) is uniform throughout.

If the laser beam delivers a homogeneous radiation, the surface heat flux is a function of the laser power (P) and the setup (Fig. 1), and can be calculated according to

$$q_s = P\frac{h_1}{h}\frac{1}{h_1' w}a, \tag{4}$$

where a is the absorptance of the surface of the material, and w is the width of the laser beam.

The *visible* nip-point is defined as the point on the substrate surface closest to the roller that receives direct radiation from the laser, which differs from the *process* nip-point (Fig. 1). Assuming the process to be steady state, the substrate surface temperature at the *visible* nip-point (T_{VNP}), can be calculated according to

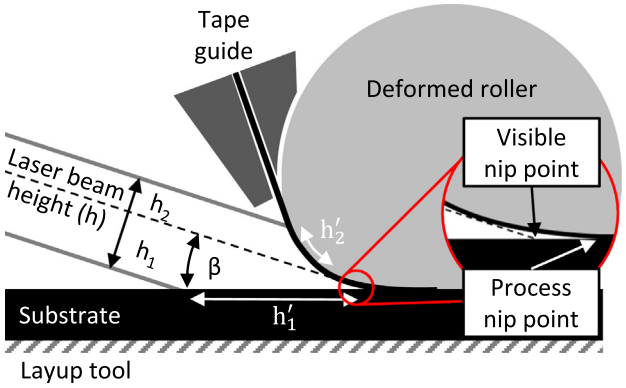

Fig. 1. Laser beam target and temperature measurement location. (For interpretation of the references to colour in this figure legend, the reader is referred to the web version of this article.)

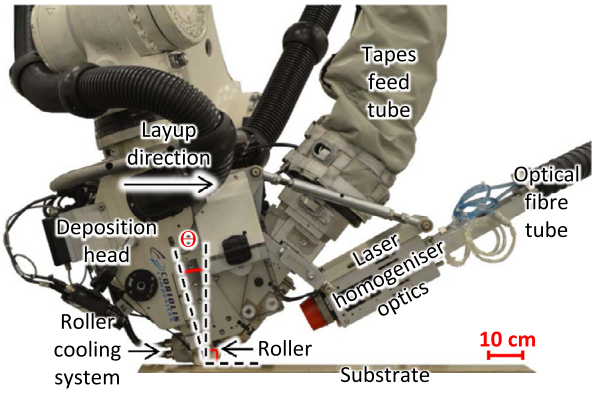

Fig. 2. Laser-assisted Coriolis Composites Automated Fibre Placement (AFP) machine head showing the installation of the laser optical unit. (For interpretation of the references to colour in this figure legend, the reader is referred to the web version of this article.)

$$T_{VNP}(P,V) = T_0 + KPV^{-0.5}; K = \overbrace{\frac{h_1}{\sqrt{h_1' wh}}}^{setup}\ \overbrace{\frac{2a}{\sqrt{\rho c_p k \pi}}}^{material}. \quad (5)$$

This expresses t as a function of the layup speed (V) and the laser heated length (h_1'). The laser power required to maintain the visible nip-point temperature constant can be determined as a function of the square root of the layup speed using

$$P(V, T_{VNP}) = AV^B; A = \frac{T_{VNP} - T_0}{K}; B = 0.5 \quad (6)$$

The proposed analytical solution of the thermal problem is simple, but based on a large number of assumptions, foremost the fact that it is only valid for a semi-infinite body.

A similar analytical solution of the problem for the case of a finite thickness body, where heat accumulation occurs, was presented by Weiler et al. [30]. The semi-infinite thickness approximation differs from the finite thickness approximation for Fourier numbers greater than approximately 0.2 ($F_0 = \alpha\, t/L^2$), with the substrate thickness L [30]. For the slowest (V = 48 mm/s) and longest heating length (70 mm heated length, 28 × 57 mm laser spot size) case considered as part of this work, the semi-infinite solid approximation is valid for substrate thicknesses L greater than 1.35 mm (9 plies) and 1.25 mm (6 plies) for the CF/PEEK and the bindered dry fibre material respectively. The solution for the finite thickness body case would be suitable to solve the thermal problem in the incoming tapes, but this is beyond the scope of the work presented in this paper.

The analytical model presented in this section will be used to guide the empirical definition of the coefficients which is presented in Section 4. The two are then compared in Section 5, which also presents a semi-empirical approach to the definition of the coefficients that reduces the number of experiments required.

3. Experimental set-up and temperature monitoring

3.1. Machine details

A state-of-the-art industrial Automated Fibre Placement machine by Coriolis Composites was used for this work (Fig. 2). The machine is capable of simultaneously laying up to eight 6.35 mm wide continuous tapes at a nominal maximum speed of 1000 mm/s. The heat source for the process is a Laserline GmbH LDF 6000–100 6 kW fibre-coupled diode laser (two diode stacks at λ = 975 ± 10 nm and two at λ = 1025 ± 10 nm). The laser is installed remotely from the fibre placement head and the beam is guided through a fibre optic cable to a homogeniser optical unit to deliver a nominally homogeneous (≈ 7 % power variation across the course width) and rectangular laser beam. Two laser homogenisers are available at the National Composites Centre, both delivering a 57 mm wide beam at the focal point, but having different laser spot heights: 8 mm and 28 mm (250 and 141 mm focal length respectively). The laser beam can be targeted by rotating the optical unit around a pivot point. The laser power can be set to a fixed value or set to vary as a continuous piecewise linear function of the deposition speed.

Other machine configuration parameters which can be adjusted and which affect the temperature distribution in the process are: the head tilt, the roller design and material, and the air pressure of the forced convection roller cooling system. These were all kept constant for the purpose of this work.

3.2. Dimensions and set-up design

Commercially available, 6.35 mm wide slit tapes were used: a carbon fibre reinforced PEEK tape (CF/PEEK) and a bindered dry-fibre tape containing 4–12 wt. % polymeric binder, both supplied by Solvay S.A. (formerly Cytec Industries Inc.). The former is coded

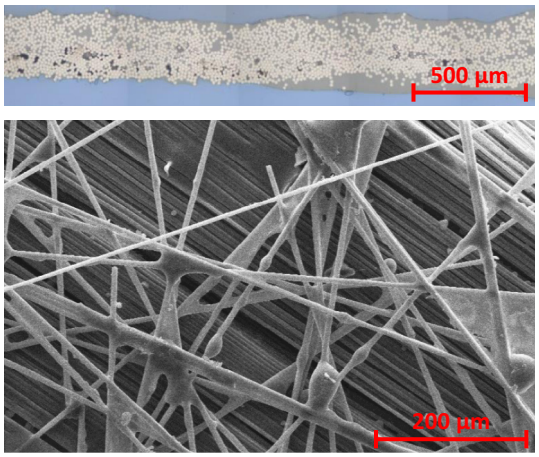

Fig. 3. Micrograph of a polished cross section of the Solvay APC-2/AS4 145/34 material (above) and scanning electron microscopy of the surface of the Solvay TX1100 material (below) as supplied by the manufacturer. (For interpretation of the references to colour in this figure legend, the reader is referred to the web version of this article.)

Table 1
Laser power distribution and laser beam angle for the 8 × 57 and the 28 × 57 mm laser spot cases.

Laser beam width (w), mm	Laser beam height (h), mm	Power split (h_1/h)	Angle (β), degree	h'_1, mm
57	8	70 %/30 %	18	18.1
57	28	85 %/15 %	20	69.6

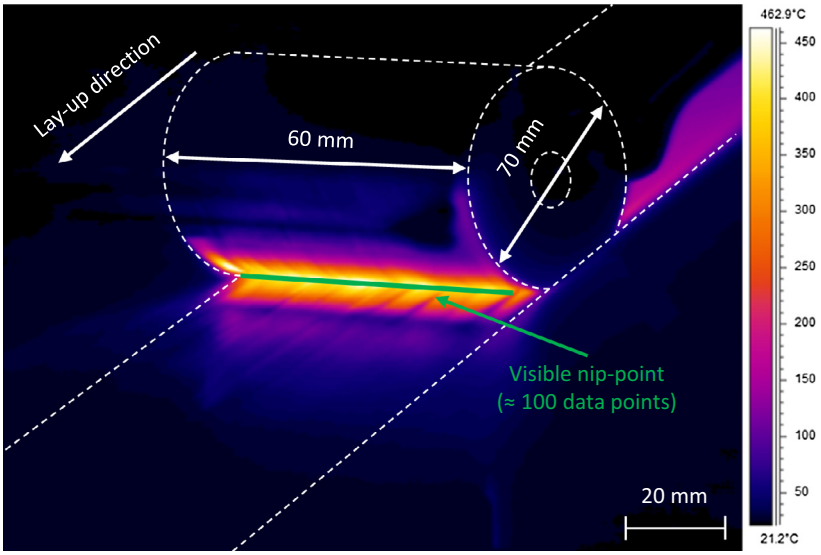

Fig. 4. Nip-point temperature measurement using a Long wave Infrared (LWIR) thermal camera. (For interpretation of the references to colour in this figure legend, the reader is referred to the web version of this article.)

APC-2/AS4 145/34 and the latter TX1100 IMS65-24K-UD-196-6.35 (Fig. 3).

Flat, unidirectional, 650 mm long test strips, made up of 8 tapes and deposited in a single 50.8 mm wide course, were laid up at a constant speed (feed and cut on the fly). Only the strips laid up at 800 mm/s were 1000 mm long and included an acceleration and deceleration region at the two ends as the feeding and cutting operation is limited to a maximum speed of 400 mm/s. The CF/PEEK strips were laid up over a 150 μm thick PEEK film (Victrex® APTIV® 1000) vacuumed to the surface of an aluminium tool. The tooling for the dry fibre test strips was prepared with a coated nylon peel ply (60 g/m^2) covered by a 50 μm thick nylon film (Airtech, Vac bag WL7400) vacuumed to the same aluminium tool.

Temperature measurements were conducted on a substrate consisting of a minimum of nine plies to minimise the effect of the heat sink into the metallic tool and the different tooling preparation. Therefore, the effect of the progressively increasing substrate thickness on the nip-point temperature can be neglected (see Section 3.4 for validation). The laminate was allowed to cool down to ambient temperature before laying up subsequent plies to ensure the same initial conditions for each test run.

Temperature measurements were conducted at four discrete layup speeds (100, 200, 400 and 800 mm/s) covering the typical deposition speed range of the Coriolis AFP machine at a range of discrete laser powers. An additional set of measurements at 48 mm/s was conducted for the CF/PEEK material only. Lower and upper laser power limits appropriate for each deposition speed and material were determined empirically to obtain a high enough temperature to adhere the new ply to the substrate without causing apparent degradation (i.e. smoke formation observed) of the incoming material and/or the roller.

A commercially available, 70 mm diameter, 40 Shore hardness silicone roller (8F14-S40SH-BL, Coriolis), recommended for the layup of materials which require a laser heater was used for this work. The compaction force was 1019 ± 42 N for the CF/PEEK and 446 ± 38 N for the dry fibre material (95 % confidence interval). Both the available laser optical units were used for this study. These were set up as described in Fig. 1 according to the parameters reported in Table 1. The deposition head tilt angle (Θ) was set to 7° backward (Fig. 2) and the pressure in the forced convection cooling system was set to 6 bar.

3.3. Surface temperature measurement set-up

The material surface temperature in the nip-point region was measured using a LWIR (λ = 7.5–13 μm) thermal camera, which operates in a different spectrum from the diode laser (λ = 0.9–1.0 μm), thus minimising the risk of the laser beam reflection in the nip-point region affecting the measurements. The camera, FLIR A325, was mounted on the placement head, to the side of the laser optical unit. The camera's IR detector has a resolution of 320 × 240 pixels (≈ 0.5 mm/pixel) and is calibrated in the 0–700 °C range to within ± 2 °C or ± 2 %, whichever is greater. All recordings were made at 30 Hz.

The camera was used to measure the temperature of the *visible* nip-point on the substrate. The visible nip-point temperature measured by the thermal camera is defined as the average temperature of the approximately 100 data-points located along an ideal line set to be parallel to the roller axis (i.e. perpendicular to the travel direction) and located at the nip-point. The temperature is sampled from 15 or more video frames (Fig. 4).

In order to obtain accurate temperature measurements, the LWIR requires the distance from the target (0.3 m), the ambient temperature (20 °C), the relative humidity (40 %) and the material emissivity to be known. The apparent emissivity of the materials when imaged at an angle of 20° to the surface in the relevant temperature range (350–450 °C for the CF/PEEK and 180 °C for the dry fibre) was determined statically in accordance to the ASTM E1933

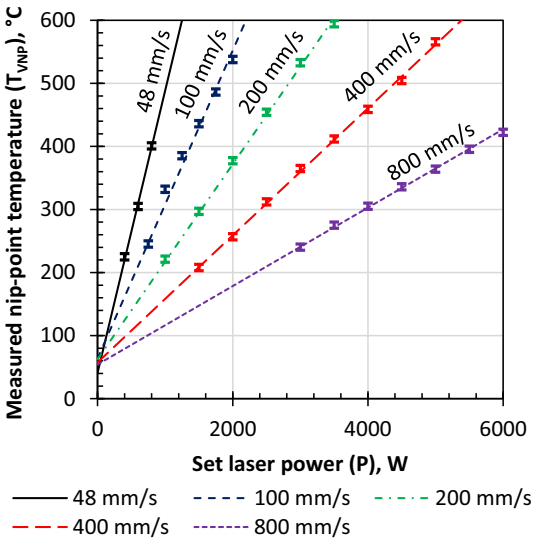

Fig. 5. Measured nip-point temperature (T) as a function of the set laser power (P) at 48, 100, 200, 400 and 800 mm/s deposition speeds. The error bars indicate 95 % confidence interval of the measurements. CF/PEEK – 8 × 57 mm laser spot shown as a representative example. (For interpretation of the references to colour in this figure legend, the reader is referred to the web version of this article.)

standard, by comparing the temperature measured by the thermal camera with that measured by a thermocouple placed in intimate contact with the material surface. The apparent emissivity is 0.80 for CF/PEEK and 0.85 for dry fibre.

Nevertheless, during layup, heat radiation from the incoming tapes may be reflected by the substrate. Consequently, the radiation detected by the camera at the visible nip-point may be a combination of radiation from the substrate and the incoming tapes. Therefore, the apparent emissivity would be higher than experimentally determined on flat laminates. This was not quantified as part of this work and contributes to the experimental uncertainty.

3.4. System capability analysis

A preliminary study was conducted using CF/PEEK to evaluate the validity of the experimental set-up described in Section 3.3, and determine the repeatability and reproducibility of the heating system and temperature measurement device combined.

In order to verify the initial assumption that the increasing substrate thickness does not affect the surface temperature, the nip-point temperature for plies 2–8 was measured at 30 equally spaced locations along the central 450 mm of a strip manufactured at a deposition speed of 48 mm/s and laser power of 1317 W to achieve a nip-point temperature of approximately 400 °C with the 28 × 57 mm laser spot. This low deposition speed, high temperature case using the largest laser spot was chosen because the heat sink in the substrate is greatest, and therefore represents the most severe case. A 77 °C temperature increase was observed between ply 2 and ply 4, but no statistically significant correlation was found between the nip-point temperature and the ply number for plies 4–8 (R^2 = 2.41E−03, p_{slope} = 0.938 » 0.05). The initial assumption that the increasing substrate thickness does not affect the nip-point temperature beyond ply 9 is valid and conservative in all cases.

In order to verify the reproducibility of the experimental set-up, the nip-point temperature for plies 2–9 was measured at 30 locations along the central 450 mm of each strip. The deposition speed was set to 400 mm/s and the laser power to 3000 W to achieve a nominal nip-point temperature of 360 °C with the 8 × 57 mm laser spot. The test was repeated three times on different days following a complete optical unit dismantling, remounting and repositioning procedure. The temperature of each set-up was determined as the average of the temperature of the 8 plies. The three measurements fell in a ± 2 °C range from the 354 °C average.

Finally, the confidence interval associated with the nip-point temperature measured at any one position from the steady state section of a unidirectional strip was determined. The standard deviation of the 30 measurements taken along the central section of each of the plies was found to be 3.2 °C on average for plies 2–9 from the three set-ups ($U_{Intra\text{-}tape}$). It should be noted that the effect of the substrate thickness (i.e. ply number) was not found to be significant for this setup.

The confidence interval associated with any single measurement was determined as the sum in quadrature of the uncertainty associated with the measurements taken along a single strip ($U_{Intra\text{-}tape}$ = ± 6.2 °C with 95 % confidence) and the uncertainty associated with the effect of the ply number ($U_{Ply\ number}$ = ± 8.4 °C with 95 % confidence) plus the uncertainty associated with the reproducibility of the experimental set-up (U_{Setup} = ± 2 °C). The overall 95 % confidence interval for the nip-point temperature is ± 12.4 °C.

Table 2
Experimentally determined regression coefficients of the nip-point temperature versus laser power linear regressions function.

Material	Setup	Deposition speed, mm/s	Slope (m), °C/W		Intercept (c), °C		R^2
			Mean	SD	Mean	SD	
CF/PEEK	8 mm high laser beam	48	0.448	3.70E−03	40.6	2.46	0.987
		100	0.244	1.10E−03	63.5	1.37	0.986
		200	0.155	5.03E−04	62.5	1.13	0.997
		400	0.101	2.65E−04	57.4	0.98	0.998
		800	0.062	5.65E−04	54.3	2.49	0.990
	28 mm high laser beam	48	0.262	1.28E−03	55.0	1.67	0.991
		100	0.158	7.74E−04	78.0	1.86	0.988
		200	0.114	4.40E−04	57.4	1.57	0.996
		400	0.064	3.32E−04	87.8	1.14	0.995
		800	0.038	1.06E−03	101.3	5.36	0.946
Dry fibre	8 mm high laser beam	100	0.498	3.23E−03	68.6	1.23	0.984
		200	0.326	2.89E−03	69.6	1.65	0.980
		400	0.252	1.21E−03	60.7	0.94	0.995
		800	0.187	2.02E−03	50.8	1.86	0.992
	28 mm high laser beam	100	0.402	4.45E−03	45.4	1.42	0.991
		200	0.272	4.23E−03	46.6	2.29	0.982
		400	0.194	1.04E−03	37.8	0.79	0.998
		800	0.129	1.00E−03	40.6	1.15	0.996

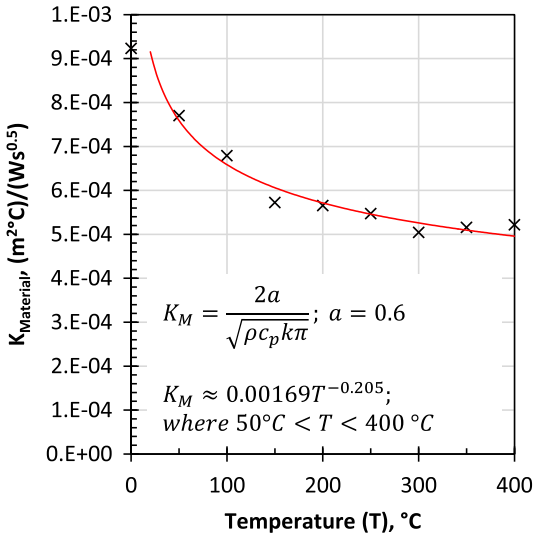

Fig. 6. Material dependent part of the coefficient K (K_M) of CF/PEEK, calculated in the 0–400 °C temperature range using the thermal properties (ρ, c_p, k) published in [32], and taking the absorptance to be 0.6 [26]. (For interpretation of the references to colour in this figure legend, the reader is referred to the web version of this article.)

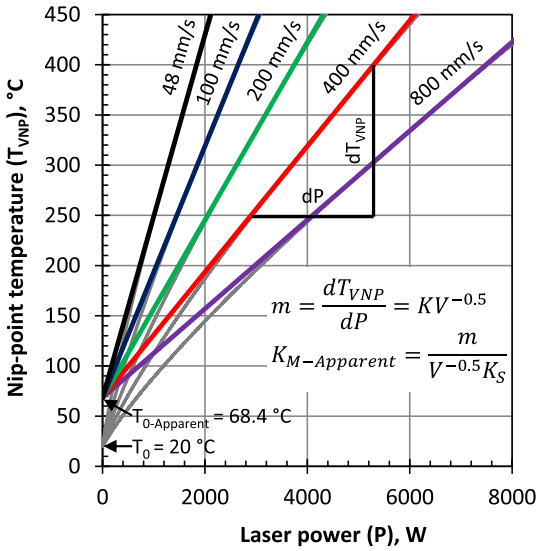

Fig. 7. Nip-point temperature as a function of the laser power for the CF/PEEK – 8 × 57 mm case, calculated using the iterative solution of the analytical model to account for the effect of the temperature on the material thermal properties (grey lines), and linear regression to the analytically determined nip-point temperature as a function of the laser power (coloured lines). (For interpretation of the references to colour in this figure legend, the reader is referred to the web version of this article.)

$$U = \sqrt{U_{Intra-tape}^2 + U_{Ply\ number}^2 + U_{Setup}^2} \quad (7)$$

The same study was conducted using a set laser power of 650 W to achieve a nominal temperature of 220 °C on the surface of the dry fibre material. The overall 95 % confidence interval for the nip-point temperature is ±17.7 °C. For the purpose of this study, these confidence intervals were applied across the entire temperature range of interest.

4. Experimental results

4.1. Empirical coefficients definition

4.1.1. Laser power dependent nip-point temperature

According to the analytical model (Eq. (5)) the visible nip-point temperatures (T_{VNP}) varies linearly with the heater power (P),

$$T_{VNP} = mP + c, \quad (8)$$

where $m = KV^{-0.5}$ and $c = T_0$. Empirically, m and c were determined by linear regression analysis to the measured visible nip-point temperatures plotted against the corresponding laser powers for each speed (Fig. 5). Standard statistical tools were used to assess the validity of the regressions [31].

The regression coefficients, m and c, were reported in Table 2 for all the tested cases together with the corresponding standard deviation (SD) and the coefficients of determination (R^2). The p-values for both the slope and the intercept were always much lower than the 0.05 threshold. As predicted by the analytical model, a strong positive correlation exists between the nip-point temperature and the laser power. It can be stated with at least 95 % confidence that the experimentally determined slope and the intercept are statistically significant (not zero).

If the analytical model was a perfect representation of reality then c would always be equal to the substrate temperature ($T_0 \approx$ 20 °C), but this was not the case. The analytical model is based on a number of assumptions, including that the material thermal properties are constant through thickness and temperature independent.

The hypothesis that the observed discrepancy between the analytical model and the regression is caused by the change in the material thermal properties (c_p, ρ, k) with temperature was tested for the case of CF/PEEK. This was done using the temperature dependent thermal properties between 0 and 400 °C reported in [32], and taking the absorptance (a) to be 0.6 at a laser angle of 20° with respect to the layup surface according to [26] (Fig. 6). The intercept of the linear regression function to the visible nip-point temperature versus laser power, converges to 68.4 °C ($T_{0\text{-}Apparent}$). The value is independent of the speed and the setup, but depends on the temperature interval selected (Fig. 7). This was calculated using Eq. (5) and an iterative solution to account for the change of thermal properties with temperature, at temperatures between 250 and 400 °C. This is congruent with what was found experimentally: 41–63 °C and 54–101 °C for the 8 × 57 and the 28 × 57 mm laser spot size respectively.

The material dependent part of the coefficient K (K_M, Eq. (5)), calculated in the 0–400 °C temperature range using the published thermal properties, increases significantly at temperatures lower than 150 °C. As a result, the visible nip-point temperature varies non-linearly with the laser power (Fig. 6). This supports the hypothesis that the observed non-linearity is caused by the change of thermal properties with temperature.

The same was found to be true for bindered dry fibre layup, for which $T_{0\text{-}Apparent}$ converges to 62.7 °C, which is congruent with what was found experimentally: 51–70 °C and 41–47 °C for the 8 × 57 and the 28 × 57 mm laser spot size respectively.

The temperature dependent density ρ(T) and specific heat capacity c_p(T) of a dry fibre bundle having a fibre volume fraction of 50 %, and ignoring the binder, were determined by rule of mixture,

$$\rho = \rho_{CF} V_f + \rho_{Air}(1 - V_f), \quad (9)$$

$$c_p = c_{p_{CF}} W_f + c_{p_{Air}}(1 - W_f). \quad (10)$$

The thermal properties of air (ρ_{Air}, c_{p_Air}, k_{Air}) at atmospheric pressure in the temperature interval of interest were sourced from [29]. The temperature dependent density of carbon fibre ρ_{CF}(T)

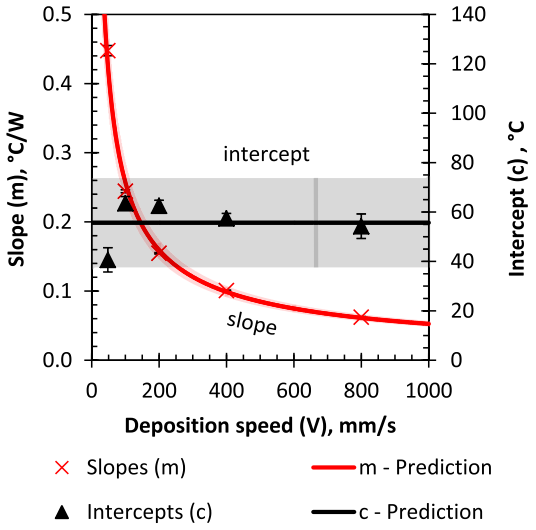

Fig. 8. Slope (m) and intercept (c) of the nip-point temperature versus set laser power linear regressions as a function of the deposition speed (V). The error bars indicate 95 % confidence interval of the coefficients. The shaded region indicates the 95 % confidence interval of the regression function. CF/PEEK – 8 × 57 mm laser spot shown as a representative example. (For interpretation of the references to colour in this figure legend, the reader is referred to the web version of this article.)

was determined from its value at room temperature (1780 kg/m^3 [33]) by using the axial and transverse coefficients of thermal expansion, −0.4E−6 and 10E−6 °C^{-1} [34]. The coefficients of thermal expansion were assumed to be constant in the temperature interval of interest. The temperature dependent heat capacity of carbon fibre $c_{p\_CF}(T)$ in the temperature range of interest was assumed to be equal to that of graphite, using data from [35]. The transverse thermal conductivity of a dry fibre bundle (k) was estimated according to the Clayton model [36],

$$k = \frac{k_{Air}}{4}\left[\sqrt{(1-V_f)^2\left(\frac{k_{CF}}{k_{Air}}-1\right)^2+\frac{4k_{CF}}{k_{Air}}}-(1-V_f)\left(\frac{k_{CF}}{k_{Air}}-1\right)\right]^2. \quad (11)$$

The temperature dependent transverse conductivity of carbon fibre $k_{CF}(T)$ could not be sourced in the literature. This was estimated from the temperature dependent axial thermal conductivity [37] assuming the ratio of the transverse (12 W/(m °C) [38]) to the axial (260 W/(m °C) [37]) thermal conductivity to be independent of temperature. The ratio of the result from Eq. (11) to the experimentally determined through-thickness thermal conductivity of a carbon fibre non-crimp fabric having a fibre volume fraction of 50 % at room temperature (0.192 W/(m °C) [39]) was used to correct the analytically determined conductivity. This was applied as a correction factor across the temperature interval assuming it to be independent of temperature. The analysis validates the hypothesis that the observed discrepancy between the analytical model and the regression to the experimental results is caused by the change of the material thermal properties with temperature.

The linear approximation to the experimental results is statistically significant, but extrapolation at low temperatures will lead to erroneous predictions as the impact of the change of thermal properties with temperature is not accounted for.

4.1.2. Deposition speed and laser power dependent nip-point temperature

According to the iterative solution of the analytical model presented in Section 4.1.1, the slope (m) of the linear function that relates the nip-point temperature to the laser power (P) varies with the deposition speed (V), $m = KV^{-0.5}$, while the intercept (c) is a constant, $c = T_{0-Apparent}$.

However, even when an iterative solution is used to account for the temperature dependent material thermal properties, this assumes those properties to be constant through the thickness, which is not the case. For a given surface temperature, the through thickness temperature distribution varies with the layup speed [30], therefore it could be envisaged that also the intercept (c) varies across the different speeds.

If both the slope (m) and the intercept (c) can be described as functions of the deposition speed, m = m(V) and c = c(V), the nip-point temperature (T_{VNP}) can be determined for any combination of V and P as

$$T_{VNP} = m(V)P + c(V). \quad (12)$$

The slopes and the intercepts which were previously determined for each of the tested speeds were plotted as a function of the deposition speed (Fig. 8).

A linear regression analysis was conducted using the least squares method to assess whether a linear function provides a good approximation of c versus V,

$$c = m_{c-V}V + c_{c-V}, \quad (13)$$

where $m_{c\text{-}V}$ and $c_{c\text{-}V}$ are the slope and the intercept of the linear regression function respectively. The intercept of the temperature versus deposition speed linear regression function (c) varies linearly with the deposition speed (V) in three of the four cases. The exception is the CF/PEEK material heated using the 8 × 57 mm laser beam size, for which the linear regression failed to define a suitable relationship between c and V (Fig. 8), i.e. no statistically significant relationship exists between c and V (R = 0.08). Therefore, in this case the slope ($m_{c\text{-}V}$) was set to zero and the intercept ($c_{c\text{-}V}$) was determined as the average of the intercepts (c) for the 5 tested deposition speeds.

According to the analytical model, the slope (m) of the nip-point temperature versus laser power regression function varies as the inverse of the square route of the layup speed (V),

$$m = A_{m-V}V^{B_{m-V}}. \quad (14)$$

where $A_{m\text{-}V} = K$ and $B_{m\text{-}V} = -0.5$. Empirically, $A_{m\text{-}V}$ and $B_{m\text{-}V}$ were determined using a least squares regression of the empirical data. The power function was found to provide a good approximation in all of the four cases tested ($R < -0.99$, $R^2 > 0.99$, $p \ll 0.05$, randomly distributed residuals). However, the exponent ($B_{m\text{-}V}$) is sig-

Table 3
Empirical coefficients and associated standard deviation.

Material	Set-up	$A_{m\text{-}V}$, °C/W		$B_{m\text{-}V}$, ln(°C/W)/ln(mm/s)		$m_{c\text{-}V}$, °C/(mm/s)		$c_{c\text{-}V}$, °C	
		Mean	SD	Mean	SD	Mean	SD	Mean	SD
CF/PEEK	8 mm high laser beam	6.15	5.37E−02	−0.689	1.59E−03	0	n/a	55.7	9.22
	28 mm high laser beam	3.74	5.35E−02	−0.679	2.79E−03	0.0559	1.66E−03	58.8	0.64
Dry fibre	8 mm high laser beam	3.97	5.51E−02	−0.460	2.29E−03	−0.0274	2.28E−03	73.2	8.15
	28 mm high laser beam	4.88	3.26E−02	−0.542	1.14E−03	−0.0086	1.16E−03	45.5	4.10

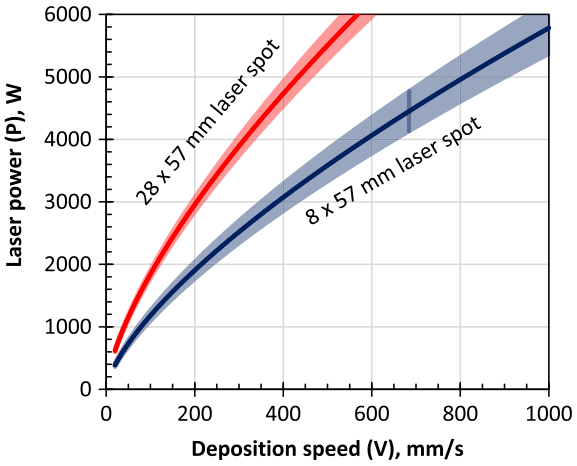

Fig. 9. Isothermal (360 °C) laser power versus deposition speed curves for CF/PEEK – 8 × 57 mm and CF/PEEK – 28 × 57 mm. The shaded region indicates the 95 % confidence interval. (For interpretation of the references to colour in this figure legend, the reader is referred to the web version of this article.)

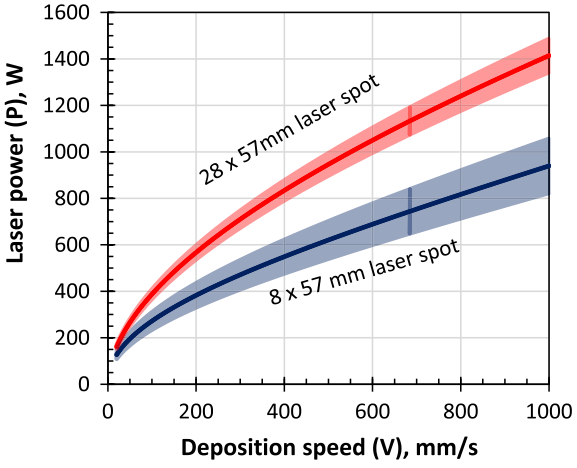

Fig. 10. Isothermal (200 °C) laser power versus deposition speed curves for dry fibre – 8 × 57 mm and dry fibre – 28 × 57 mm (95 % confidence interval shown). The shaded region indicates the 95 % confidence interval. (For interpretation of the references to colour in this figure legend, the reader is referred to the web version of this article.)

nificantly lower than −0.5 for the case of CF/PEEK (≈ −0.7 for the case of CF/PEEK).

The discrepancy between the empirically determined exponents (≈ −0.7 for the case of CF/PEEK), and what would be expected according to the analytical model (−0.5), can be traced back to the effect of the layup speed on the through thickness temperature distribution [40] and its effect on the material thermal properties.

Within the limits of the tested configuration and combination of setup values, the nip-point temperature can be determined according to

$$T_{VNP} = mP + c,$$

where

$$m = A_{m-V} V^{B_{m-V}} \tag{15}$$

and

$$c = m_{c-V} V + c_{c-V}.$$

The laser power required to maintain a constant nip-point temperature across a range of speeds can be determined by rearranging Eq. (15) to obtain

$$P(W) = AV^B;\ A = \frac{T_{VNP} - (m_{c-V} V + c_{c-V})}{A_{m-V}};\ B = -B_{m-V}. \tag{16}$$

The empirically determined machine set-up and material specific regression coefficients which were determined as part of this study are reported in Table 3. These were used to calculate the laser power required to maintain a constant nip-point temperature according to Eq. (16), and the results reported in Figs. 9 and 10. The confidence interval was determined using the Monte Carlo method.

4.2. Empirical coefficients validation

The regression coefficients were determined empirically by conducting steady-state measurements at different power and speed levels. It is the purpose of this section to demonstrate that these can be used to control the temperature during variable speed deposition. Bur et al. [41] shows through numerical modelling that an error is committed when controlling the heater power using parameters derived from a steady state solution. This was not shown experimentally and does not take into account the additional error occurring because of the response time of the heater control system.

In order to validate the applicability of the empirically determined coefficients to a variable speed layup, a 1500 mm long, one course wide, unidirectional strip was laid up. The machine was programmed to feed the material at 200 mm/s, accelerate to 800 mm/s in the layup region and decelerate down to 400 mm/s at cut. The acceleration was set to 500 mm/s^2 and the deceleration was set to 1000 mm/s^2. These were chosen to be representative of the layup of a geometrically simple part.

The validation was carried out using the 8 × 57 mm spot size lens, and the results are reported in Fig. 11 for CF/PEEK and Fig. 12 for Dry Fibre. At the time when the tests were conducted, the Coriolis AFP machine installed at the NCC could only control the laser power as a linear function of the deposition speed. To accommodate this constraint, the non-linear relationship was approximated linearly over the 200–800 mm/s range (Table 4). Three nominal temperatures were tested for each material.

The nip-point temperature was monitored as outlined in Section 3.3. The measured temperature for each of the three strips was plotted as a function of the position along the strip (Figs. 11 and 12). The predicted nip-point temperature was determined from the deposition speed and the programmed laser power at each point along the strip according to Eq. (15) and using the regression coefficients given in Table 3 and plotted in Figs. 11 and 12. The upper and lower bounds for the prediction were determined using the Monte Carlo method.

For each of the six datasets, an Anderson-Darling normality test (AD) was conducted to determine whether the difference between the predicted and the measured values (the residuals) follows a normal distribution. The mean residual (the model bias) is always lower than 7 % of the nominal temperature and less than 2 % in most cases. The p-value is always greater than the 0.05 threshold and the AD coefficient is always small (AD < 0.7) (Table 5). This demonstrates that thermal coefficients determined by conducting steady-state measurements can be used to define the laser control parameters for variable speed layup with accelerations of up to ±1 m/s^2.

This shows that the material can be laid up successfully by controlling the laser power as a linear function of the layup speed in the 200–800 mm/s layup speed range. The temperature deviation from the target introduced because of the linear control function

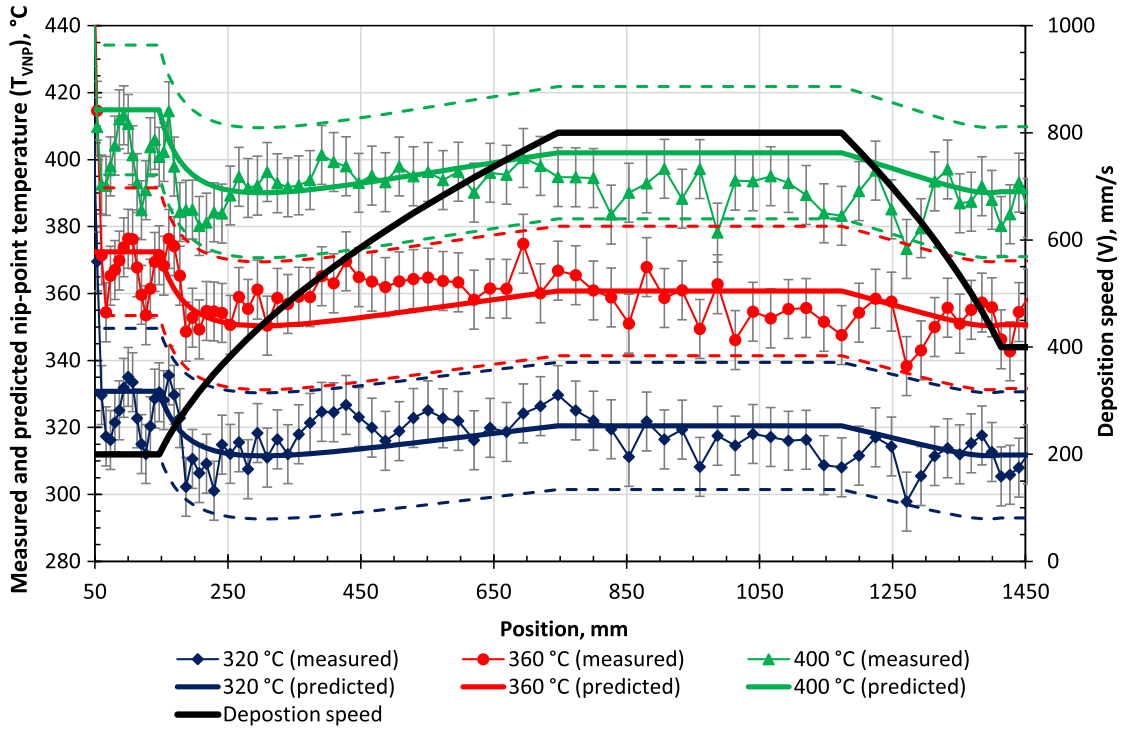

Fig. 11. Process model validation for CF/PEEK – 8 × 57 mm showing good correlation between the measurements and the prediction with less than 2 % bias. The error bars indicate 95 % confidence interval of the measurements. The dashed lines indicate the 95 % confidence interval of the prediction. (For interpretation of the references to colour in this figure legend, the reader is referred to the web version of this article.)

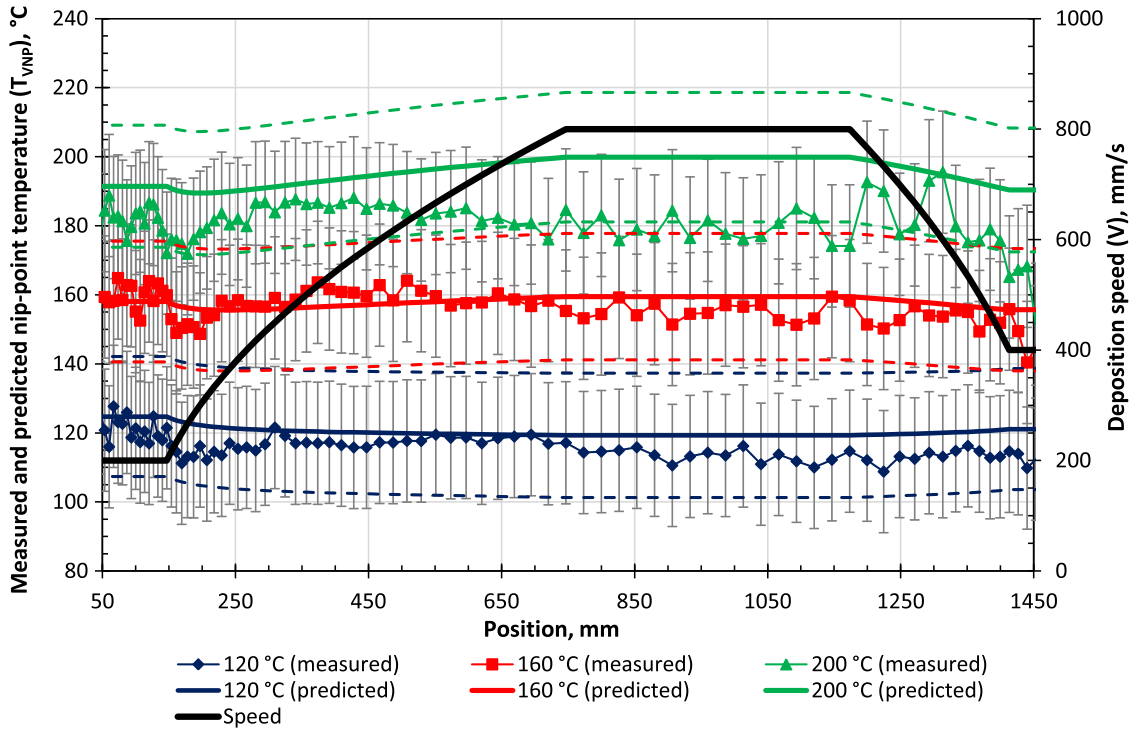

Fig. 12. Process model validation for dry fibre – 8 × 57 mm showing good correlation between the measurements and the prediction with less than 7 % bias. The error bars indicate 95 % confidence interval of the measurements. The dashed lines indicate the 95 % confidence interval of the prediction. (For interpretation of the references to colour in this figure legend, the reader is referred to the web version of this article.)

did not exceed 15 °C in any of the cases considered (Figs. 11 and 12). A linear approximation is only valid for relatively narrow layup speed ranges and/or high layup speeds.

In order to demonstrate the need for a non-linear control function during variable speed layup across a wide speed range including very low speeds, another CF/PEEK, 1500 mm long, one course

Table 4
Laser power linear control parameters.

Layup speed range, mm/s	Material	Target temperature, °C	Power at 0 mm/s, W	Power at 800 mm/s, W
200–800	CF/PEEK	320	859	4304
		360	988	4962
		400	1118	5636
	Dry fibre	120	95	375
		160	750	595
		200	205	816
20–800	CF/PEEK	360	716	5107

Table 5
Mean, standard deviation and normality test results for the residuals of the empirical model validation.

Material	Nominal temperature, °C	Mean, °C	Standard Deviation, °C	AD (AD < 0.7)	P (p > 0.05)
CF/PEEK	320	0.6	8.7	0.502	0.200
	360	−1.1	9.3	0.466	0.247
	400	6.6	8.5	0.455	0.262
Dry fibre	120	5.0	3.0	0.096	0.997
	160	1.2	4.4	0.273	0.659
	200	13.2	6.5	0.675	0.075

wide, unidirectional strip was laid up. In this case the machine was programmed to feed the material at 20 mm/s, accelerate to 800 mm/s in the layup region and decelerate down to 400 mm/s at cut. The acceleration and the deceleration were both set to 800 mm/s^2. These were chosen to be representative of the layup of a geometrically complex part. The same procedure was repeated in the 20–800 mm/s deposition speed range with a target temperature of 360 °C, see Table 4 for the control parameters. The predicted temperature at 20 mm/s was 700 ± 21 °C, the measured temperature at this speed was 696 ± 7.9 °C and the material was visibly degraded.

This test demonstrates clearly the need for a non-linear control function when laying up the material across a wide range of speeds. Although this was only shown for one material type at one temperature, the good correlation between predicted and measured values at 20 mm/s show that the empirical model is robust.

5. Analytical coefficients validation and semi-empirical coefficients definition

Section 4 presents and validates a procedure to determine the four coefficients of the model empirically, $A_{m\text{-}V}$, $B_{m\text{-}V}$, $m_{c\text{-}V}$, $c_{c\text{-}V}$. These were used as the reference against which the analytical and the semi-empirical coefficients were validated.

The correlation coefficient (R_T) was defined as

$$R_T = \frac{[T_{Empirical}(P_{T_{Target}}, V)] - T_0}{T_{Target} - T_0} \quad (17)$$

where T_{Target} is the target visible nip-point temperature, in this case set to 360 °C for CF/PEEK and 160 °C for dry fibre. $T_{Empirical}$ is the nip-point temperature calculated according to Eq. (15) using the empirically determined coefficients (Table 3) at the power level required to achieve the target temperature (P_{T_Target}), calculated using the set of coefficients to be validated, analytical or semi-empirical. T_0 is ambient temperature (20 °C).

The analytical coefficients were determined as follows and were reported in Table 7. $A_{m\text{-}V}$ is the product of the setup (K_S) and the material (K_M) dependent part of the coefficient K. The former, K_S, was calculated according to Eq. (5) using the parameters reported in Table 1 (91.2 and 56.5 m$^{-1.5}$ respectively for the 8 × 57 and the 28 × 57 mm laser spot cases). The latter, K_M, was calculated according to Eq. (5) using the material thermal properties reported in Table 6 (5.17E−4 and 1.33E−3 m^2°C/(Ws$^{0.5}$) for CF/PEEK at 360 °C and dry fibre at 50 % fibre volume fraction and 160 °C respectively). $B_{m\text{-}V}$ is equal to −0.5, $m_{c\text{-}V}$ is equal to zero, and $c_{c\text{-}V}$ is equal to the initial temperature of the substrate (T_0 = 20 °C).

Table 6
Material thermal properties.

	CF/PEEK at 360 °C	Dry Fibre at V_f^* = 0.5 and 160 °C
Density (ρ), kg/m^3	1660 [32]	888[a]
Specific heat capacity (c_p), J/(kg °C)	1534 [32]	1090[b]
Conductivity (k), W/(m °C)	0.67 [32]	0.268[c]
Absorptance (a)	0.6 at β = 20 °C [26]	

[a] Determined according to Eq. (9) as outlined in Section 4.1.1 with data from [29,33,34].
[b] Determined according to Eq. (10) as outlined in Section 4.1.1 with data from [29,35].
[c] Determined according to Eq. (11) as outlined in Section 4.1.1 with data from [29,37–39].

A revised version of the analytical coefficients (iterative analytical) was also compared with the empirical ones. These were determined in the same way as the analytical ones, with two exceptions. $c_{c\text{-}V}$ is not equal to the initial temperature of the substrate, but it is equal to the intercept of the linear regression function to the surface temperature versus power determined iteratively ($T_{0\text{-}Apparent}$ = 68.4 °C for CF/PEEK and $T_{0\text{-}Apparent}$ = 65.8 °C for dry fibre). K_M is equal to the slope of the same function ($K_{M\text{-}Apparent}$ equals 4.34E−4 and 9.23E−4 (m^2°C)/(Ws$^{0.5}$) for CF/PEEK and dry fibre respectively). These were also reported in Table 7.

The correlation (Eq. (17)) of the model calculated with the analytical and iterative analytical coefficients is poor (Fig. 13). This could be traced back to two broad causes: (1) the fact that the analytical coefficients were based on a number of fundamental assumptions that do not hold true in this case (e.g. the material thermal properties are assumed to be constant through the thickness), and (b) the material thermal properties which were sourced in the literature are not representative of the properties of the tested materials.

However, a set of semi-empirical set of coefficients could be defined which can be determined with reduced experimental effort. The following was hypothesised, and then tested:

Table 7
Empirical, analytical and semi-empirical coefficients.

		Empirical	Analytical	Analytical iterative	Semi empirical 1	Semi empirical 2	
CF/PEEK, T_{VNP} = 360 °C	8 × 57 mm	6.15	1.49	1.25	5.26	4.20	$A_{m\text{-}V}$
		−0.689	−0.500	−0.500	−0.668	−0.604	$B_{m\text{-}V}$
		0.00	0.00	0.00	0.00	0.00	$m_{c\text{-}V}$
		55.7	20.0	68.4	68.4	68.4	$c_{c\text{-}V}$
	28 × 57 mm	3.74	0.92	0.78	2.60	3.26	$A_{m\text{-}V}$
		−0.679	−0.500	−0.500	−0.604	−0.668	$B_{m\text{-}V}$
		0.06	0.00	0.00	0.00	0.00	$m_{c\text{-}V}$
		58.8	20.0	68.4	68.4	68.4	$c_{c\text{-}V}$
Dry fibre, $T_{VN}P$ = 160 °C	8 × 57 mm	3.97	3.83	2.66	6.32	7.05	$A_{m\text{-}V}$
		−0.460	−0.500	−0.500	−0.543	−0.554	$B_{m\text{-}V}$
		−0.03	0.00	0.00	0.00	0.00	$m_{c\text{-}V}$
		72.2	20.0	65.8	65.8	65.8	$c_{c\text{-}V}$
	28 × 57 mm	4.88	2.38	1.65	4.37	3.92	$A_{m\text{-}V}$
		−0.542	−0.500	−0.500	−0.554	−0.543	$B_{m\text{-}V}$
		−0.01	0.00	0.00	0.00	0.00	$m_{c\text{-}V}$
		45.5	20.0	65.8	65.8	65.8	$c_{c\text{-}V}$

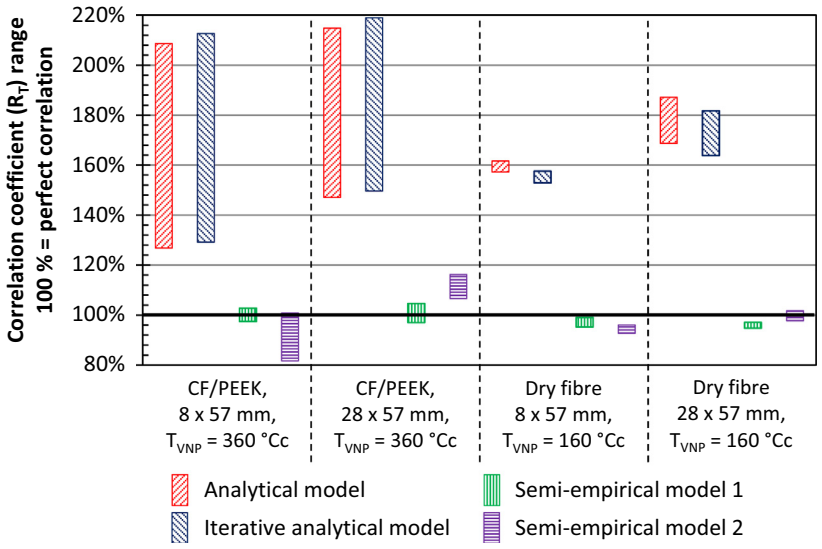

Fig. 13. Analytical and semi-empirical models validation. (For interpretation of the references to colour in this figure legend, the reader is referred to the web version of this article.)

- $c_{c\text{-}V}$ (= $T_{0\text{-}Apparent}$) is a material dependent parameter. If the temperature dependent thermal properties of the material are known, this can be determined through an iterative solution of the analytical model.
- $m_{c\text{-}V}$ is always equal to zero.
- $B_{m\text{-}V}$ is a material dependent parameter, albeit one which is currently not linked with the material thermal properties, and needs to be determined experimentally by measuring the nip-point temperature at one power level at three layup speeds (lowest, intermediate, highest)
- $A_{m\text{-}V}$ (= K_S $K_{M\text{-}Apparent}$ ϕ) is a material and setup dependent parameter, with a material specific correction factor (ϕ) which needs to be determined experimentally from the same tests outlined for $B_{m\text{-}V}$.

Therefore, defining the coefficients for a new material and machine setup requires the temperature dependent thermal properties of the material to determine $T_{0\text{-}Apparent}$ and $K_{M\text{-}Apparent}$. It also requires the measured nip-point temperature at three combinations of the laser power and layup speed to determine $B_{m\text{-}V}$ and ϕ (semi-empirical 1, Table 7).

Moreover, defining the coefficients for an alternative machine setup of the same material (e.g. 8 × 57 to 28 × 57 mm laser spot size, or vice versa) requires no additional testing. $A_{m\text{-}V}$ can be corrected to account for the different heating area by changing the setup dependent part of the coefficient K (K_S) and using the material specific correction factor (ϕ). The other parameters ($B_{m\text{-}V}$, $m_{c\text{-}V}$, $c_{c\text{-}V}$) are material specific and do not change with the setup (semi-empirical 2, Table 7).

This was tested for both CF/PEEK and dry fibre. $B_{m\text{-}V}$ and φ were determined by fitting the model to the measured nip-point temperature at the intermediate power level tested for each of the lowest (48 and 100 mm/s for CF/PEEK and dry fibre respectively), intermediate (400 mm/s), and highest (800 mm/s) speed. Furthermore, the measured nip-point temperature at the lowest and the highest laser power tested for each of the three layup speeds was also considered to determine the sensitivity of the coefficients to the selection of the experimental points. The points which were used to determine the semi-empirical coefficients 1 were reported in Table 8, the regression coefficients were reported in Table 7, and the correlation coefficients in Fig. 13.

The correlation (Eq. (17)) of the model calculated with both sets of semi-empirical coefficients is good (Fig. 13). The maximum error ($|1 - R_T|$) was 5 % for the semi-empirical coefficients 1, which can be defined with three tests only, and 18 % for the semi-empirical coefficients 2, which can be defined with no additional tests for an alternative setup to one which is already characterised.

Table 8
Experimental points used to determine the semi-empirical coefficients ($A_{m\text{-}V}$ and $B_{m\text{-}V}$) and to assess their sensitivity to the selection of the experimental points.

Material	Layup speed, mm/s	8 × 57 mm			28 × 57 mm		
		Power, W/Temperature, °C			Power, W/Temperature, °C		
		Low	Mid	High	Low	Mid	High
CF/PEEK	48	400/225	600/305	800/401	750/253	1250/382	1750/507
	400	1500/208	3500/412	5500/611	2000/215	3500/310	4500/377
	800	2500/205	4500/336	6000/422	4000/249	5000/298	6000/323
Dry fibre	100	150/138	350/248	550/338	250/150	350/186	450/225
	400	350/146	650/224	1100/334	650/166	650/166	1050/239
	800	450/132	850/209	1300/288	850/148	1100/187	1600/246

Furthermore, within the range of available experimental data, the semi-empirical coefficients showed limited sensitivity to the selection of the power level. When selecting the lowest/highest laser power available at each speed, the maximum error increased from 5 % to 9 % for the semi-empirical 1 case, and from 18 % to 24 % for the semi-empirical 2 case. These are rather extreme cases as the power level selected corresponds to the tapes barely tacking (lowest) or to visible degradation occurring (highest). The procedure is robust.

A semi-empirical approach to the definition of the coefficients was derived from the analytical one and validated successfully against the empirical one. The semi-empirical approach is robust and reduces the experimental effort required to determine the coefficients of the model significantly.

6. Discussion

An analytical, an empirical, and a semi-empirical approach to the determination of the coefficients that define the relationship between the visible nip-point temperature, the laser power, and the deposition speed was proposed.

The empirical coefficients were successfully validated in the 200–800 mm/s deposition speed range for both a carbon fibre reinforced thermoplastic prepreg and a bindered dry fibre material. The residuals are always randomly distributed showing that the temperature is correctly predicted across the entire deposition speed range during variable speed layup. The bias is low, less than 2 % of the measured temperature for the CF/PEEK material and less than 7 % for the dry fibre material.

The prediction confidence intervals are much larger for the dry fibre material (≈ ± 12 %) than for the CF/PEEK material (≈ ± 5 %). This can be traced back to the reported lack of accuracy and repeatability of the laser at power levels lower than approximately 10 % of the maximum output power [13] and to the larger variability expected from the as supplied dry fibre material in comparison with the preconsolidated CF/PEEK prepreg. These may also indicate why the calculated measurement confidence interval (Section 3.4) is larger for the dry fibre material (± 18 °C) than for the CF/PEEK one (± 12 °C). In order to improve the prediction and temperature control accuracy, the maximum power of the laser should be tailored to the material specific power requirements, so that the 10% lower threshold is not exceeded at the slowest deposition speeds of interest.

However, the proposed experimental procedure and data processing method is time consuming, and, for any variation, a new set of coefficients needs to be determined experimentally. Therefore, a semi-empirical approach to the definition of the coefficients and associated simplified experimental procedure was derived to reduce the number of experiments required, and to address the limits of the analytical approach which was shown to over predict the required leaser power significantly.

The proposed semi-empirical approach enables defining the parameters with three tests only (one laser power at three speeds), while correlating to within 5 % of the empirical approach, which requires about 20 individual combinations to be tested (4 laser powers at 5 speeds). Furthermore, it was shown that, if the configuration only is changed, and not the material, the parameters for the new configuration (e.g. different laser spot size), can be determined without any additional test, and causing an 18 % temperature error in the worst case. The sensitivity of the model to the selection of the test point was found to be low, leading to a robust procedure.

The proposed semi-empirical approach to the definition of the model coefficients, and associated experimental procedure, constitute a step change from current industrial trial and error practices as it allows defining the speed dependent heater power as well as predicting the nip-point temperature. It also constitutes a significant improvement with respect to the empirical approach as it requires a significantly reduced number of tests.

However, there are a number of limitations associated with the open-loop temperature control approach, regardless of how the control parameters are determined, analytical, numerical, empirical, or semi-empirical.

- The relative angle between the top ply of the substrate and the ply which is being laid up may affect the heating process. A specific set of parameters for each relative angle of interest (0°, 45° and 90° in most cases) may be required.
- The substrate is assumed to be at constant temperature. This may not be a valid assumption for the case of a small preform laid up using a large heated area at high temperature. A substrate temperature dependent set of parameters may need to be determined.
- The ply number (i.e. preform thickness), was shown not to affect the surface temperature from ply 4 onward. Therefore, the layup of the first three plies requires bespoke parameters if the temperature is to be kept constant.
- The open-loop temperature control system could be difficult to apply to the layup of geometrically complex parts.

Furthermore, there are a number of limitations associated with any control system which is based on controlling surface temperature, regardless of whether it is closed or open loop. In the case of a CF/PEEK preform laid up using a laser-assisted AFP machine, the thermal history of the material during the process, the preform meso-structure, and the preform interlaminar shear strength, vary with the layup speed, despite of the nip-point temperature being constant [16,42]. Furthermore, [43] showed that the thermal history of the material during the process and the preform meso-structure vary with the size of the laser heated area, despite of the laser power being controlled to obtain the same nip-point temperature in both cases.

These evidences suggest that nip-point temperature alone is not sufficient to control the process. A deposition speed dependent heater power function delivering a constant material state at the end of the process (e.g. constant void content and crystallinity for the thermoplastic case, and constant preform fibre volume fraction for the dry fibre case), rather than a constant nip-point temperature, may need to be developed through robust numerical modelling of the entire process and/or experiments. A step in this direction was taken by Khan et al. [44] who presented numerically determined curves for the HGT's gas volume required to achieve constant degree of inter-ply bonding and void content for CF/PEEK laid up at speeds between 50 and 167 mm/s.

7. Conclusions and further work

Automated Fibre Placement requires accurate control of the heater power to deposit the material at appropriate temperatures throughout the process. This paper presents a validated semi-empirical model, and the associated experimental procedure and data reduction method, to determine the speed dependent heater power function required to maintain the substrate surface temperature constant during variable speed layup. The model is based on simple measurements of the surface temperature during steady state layup for a range of heater powers and layup speeds. This approach enables open-loop control of the heater power as a function of the layup speed.

Future work will address the limitations of the semi-empirical approach, of the open-loop heater control system, and of the surface temperature control approach. The semi-empirical approach will be validated against a wider range of materials, heater types and machine setting to further validate its applicability and to standardise the procedure to enable reproducible results. The effect of the ply relative orientation, of the preform temperature, and of the tool geometry on the validity of the open-loop control system will be further investigated, and bespoke control parameters determined if necessary.

Acknowledgements

This work was supported by the National Composites Centre Core Research and Technology Programmes (www.nccuk.com). Many discussions on thermal management with Dr Peter Giddings and the contribution of Ed Goodman and Matt Scott of the National Composites Centre are kindly acknowledged. Mattia Di Francesco and Laura Veldenz would like to acknowledge the support of the Engineering and Physical Sciences Research Council through the EPSRC Centre for Doctoral Training in Composites Manufacture [EP/K50323X/1]. Due to commercial partner restrictions the underlying data for this paper cannot be shared.

References

[1] Lukaszewicz DHJA, Ward C, Potter KD. The engineering aspects of automated prepreg layup: history, present and future. Compos Part B Eng 2012;43:997–1009. http://dx.doi.org/10.1016/j.compositesb.2011.12.003.
[2] Comer AJ, Ray D, Obande WO, Jones D, Lyons J, Rosca I, et al. Mechanical characterisation of carbon fibre-PEEK manufactured by laser-assisted automated-tape-placement and autoclave. Compos Part A Appl Sci Manuf 2015;69:10–20. http://dx.doi.org/10.1016/j.compositesa.2014.10.003.
[3] Di Francesco M, Veldenz L, Koutsomitopoulou A, Dell'Anno G, Potter K. On the development of multi-material automated fibre placement technology. In: Int. Conf. Manuf. Adv. Compos., Bristol, UK.
[4] Lukaszewicz DHJA, Potter KD, Eales J. A concept for the in situ consolidation of thermoset matrix prepreg during automated lay-up. Compos Part B Eng 2013;45:538–43. http://dx.doi.org/10.1016/j.compositesb.2012.09.008.
[5] Veldenz L, Di Francesco M, Astwood S, Dell'Anno G, Kim BC, Potter K. Characteristics and processability of bindered dry fibre material for automated fibre placement. In: 17th Eur. Conf. Compos. Mater., Munich, DE.
[6] Hörmann P, Stelzl D, Lichtinger R, Van Nieuwenhove S, Mazón Carro G, Drechsler K. On the numerical prediction of radiative heat transfer for thermoset automated fiber placement. Compos Part A Appl Sci Manuf 2014;67:282–8. http://dx.doi.org/10.1016/j.compositesa.2014.08.019.
[7] Lukaszewicz DH-JA, Potter K. Through-thickness compression response of uncured prepreg during manufacture by automated layup. Proc Inst Mech Eng Part B J Eng Manuf 2011;226:193–202. http://dx.doi.org/10.1177/0954405411411811.
[8] Grouve WJB, Warnet LL, Rietman B, Akkerman R. On the weld strength of in situ tape placed reinforcements on weave reinforced structures. Compos Part A Appl Sci Manuf 2012;43:1530–6. http://dx.doi.org/10.1016/j.compositesa.2012.04.010.
[9] Comer AJ, Ray D, Hammond P, Lyons J, Obande WO, Jones D. Wedge Peel interlaminar toughness of carbon-fibre/PEEK thermoplastic laminates manufactured by Laser Assisted Automated Tape Placement (LATP). Tampere, FI: SAMPE Eur. - SETEC; 2014.
[10] Matveev MY, Schubel PJ, Long AC, Jones IA. Understanding the buckling behaviour of steered tows in Automated Dry Fibre Placement (ADFP). Compos Part A Appl Sci Manuf 2016;90:451–6. http://dx.doi.org/10.1016/j.compositesa.2016.08.014.
[11] Mantell SC, Springer GS. Manufacturing process models for thermoplastic composites. J Compos Mater 1992;26:2348–77. http://dx.doi.org/10.1177/002199839202601602.
[12] Qureshi Z, Swait T, Scaife R, El-Dessouky HM. In situ consolidation of thermoplastic prepreg tape using automated tape placement technology: potential and possibilities. Compos Part B Eng 2014;66:255–67. http://dx.doi.org/10.1016/j.compositesb.2014.05.025.
[13] Stoffers N, Krombholz C. Efficient production of wing shells in dry fiber placement. In: 17th Eur. Conf. Compos. Mater. (ECCM17), Munich, DE.
[14] Laserline. Diode laser manual; 2012.
[15] Heraeus Noblelight. Carbon infrared emitter CIR® n.d <https://www.heraeus.com/en/landingspages/lp_hng/heraeus_infrared_heat_solutions/products_and_solutions_2/carbon_infrared_emitters_uk.aspx> (accessed January 30, 2017).
[16] Stokes-Griffin CM, Compston P. The effect of processing temperature and placement rate on the short beam strength of carbon fibre-PEEK manufactured using a laser tape placement process. Compos Part A Appl Sci Manuf 2015;78:274–83. http://dx.doi.org/10.1016/j.compositesa.2015.08.008.
[17] Hassan N, Thompson JE, Batra RC, Hibler AB, Song Xiaolan, Loos AC. A heat transfer analysis of the fiber placement composite manufacturing process. J Reinf Plast Compos 2005;24:869–88. http://dx.doi.org/10.1177/0731684405047773.
[18] Skandali M, Jansen K, Koussios S, Sinke J, Benedictus R. Two-dimensional and transient thermal model of the continuous tape laying process. In: 20th Int. Conf. Compos. Mater., Copenhagen, DK.
[19] Stokes-Griffin CM, Compston P, Matuszyk TI, Cardew-Hall MJ. Thermal modelling of the laser-assisted thermoplastic tape placement process. J Thermoplast Compos Mater 2013;28:1445–62. http://dx.doi.org/10.1177/0892705713513285.
[20] Stokes-Griffin CM, Compston P. A combined optical-thermal model for near-infrared laser heating of thermoplastic composites in an automated tape placement process. Compos Part A Appl Sci Manuf 2015;75:104–15. http://dx.doi.org/10.1016/j.compositesa.2014.08.006.
[21] Colton J, Leach D. Processing parameters for filament winding thick-section PEEK/carbon fiber composites. Polym Compos 1992;13:427–34. http://dx.doi.org/10.1002/pc.750130605.
[22] Tierney J, Gillespie JW. Modeling of in situ strength development for the thermoplastic composite tow placement process. J Compos Mater 2006;40:1487–506. http://dx.doi.org/10.1177/0021998306060162.
[23] Grouve WJB. Weld strength of laser-assisted tape-placed thermoplastic composites. University of Twente; 2012.
[24] Narnhofer M, Pazour P, Schledjewski R. CFD simulations of a hot gas torch for the thermoplastic tape placement process. In: 15th Eur. Conferece Compos. Mater., Venice, IT.
[25] Grove SM. Thermal modelling of tape laying with continuous carbon fibre-reinforced thermoplastic. Composites 1988;19:367–75. http://dx.doi.org/10.1016/0010-4361(88)90124-3.
[26] Stokes-Griffin CM, Compston P. Optical characterisation and modelling for oblique near-infrared laser heating of carbon fibre reinforced thermoplastic composites. Opt Lasers Eng 2015;72:1–11. http://dx.doi.org/10.1016/j.optlaseng.2015.03.016.
[27] Levy A, Heider D, Tierney J, Gillespie JW. Inter-layer thermal contact resistance evolution with the degree of intimate contact in the processing of thermoplastic composite laminates. J Compos Mater 2013;48:491–503. http://dx.doi.org/10.1177/0021998313476318.
[28] Tierney J, Gillespie JW. Modeling of heat transfer and void dynamics for the thermoplastic composite tow-placement process. J Compos Mater 2003;37:1745–68. http://dx.doi.org/10.1177/0021998303035188.
[29] Cengel YA. Heat and mass transfer: a practical approach. 3rd ed. New York, NY: McGrawn-Hill; 2007.
[30] Weiler T, Emonts M, Wollenburg L, Janssen H. Transient thermal analysis of laser-assisted thermoplastic tape placement at high process speeds by use of analytical solutions. J Thermoplast Compos Mater 2017. http://dx.doi.org/10.1177/0892705717697778. 089270571769778.
[31] Bass I. Six sigma statistics with excel and minitab. New York, US: McGrawn-Hill; 2007.
[32] Cogswell FN. Thermoplastic aromatic polymer composites: a study of the structure, processing, and properties of carbon fibre reinforced

polyetheretherketone and related materials. Oxford, UK: Butterworth-Heinemann; 1992.
[33] TohoTenax. TENAX®- E IMS65 E23 24K 830tex 2011.
[34] Hull D, Clyne TW. An introduction to composite materials. Cambridge, UK: Cambridge University Press; 1996.
[35] Yang J, Roy C. Using DTA to quantitatively determine enthalpy change over a wide temperature range by the "mass-difference baseline method". Thermochim Acta 1999;333:131–40. http://dx.doi.org/10.1016/S0040-6031(99)00106-9.
[36] Dasgupta A, Agarwal RK. Orthotropic thermal conductivity of plain-weave fabric composites sing a homogenization technique. J Compos Mater 1992;26:2736–58.
[37] Wang J, Gu M, Ma W, Zhang X, Song Y. Temperature dependence of the thermal conductivity of individual pitch-derived carbon fibers. New Carbon Mater 2008;23:259–63. http://dx.doi.org/10.1016/S1872-5805(08)60029-3.
[38] Huang HS, Ganguli S, Roy AK. Prediction of the transverse thermal conductivity of pitch-based carbon fibers. J Compos Mater 2013;48:1383–90. http://dx.doi.org/10.1177/0021998313486501.
[39] Yang Y, Robitaille F, Hind S. Thermal conductivity of carbon fiber fabrics. In: 19th Int. Conf. Compos. Mater., Montreal, CA.
[40] Weiler T, Emonts M, Striet P, Gronenborn S, Janssen H. Optical modelling of VCSEL-assisted thermoplastic tape placement. In: 17th Eur. Conf. Compos. Mater., Munich, DE.
[41] Bur N, Joyot P, Ghnatios C, Villon P, Cueto E, Chinesta F. On the use of model order reduction for simulating automated fibre placement processes. Adv Model Simul Eng Sci 2016;3:4. http://dx.doi.org/10.1186/s40323-016-0056-x.
[42] Di Francesco M, Valverde MA, Ward C, Giddings PF, Dell' Anno G, Potter K. Influence of layup speed on the quality of thermoplastic preforms manufactured by laser-assisted automated fibre placement. In: 17th Eur. Conf. Compos. Mater. (ECCM17), Munich, DE.
[43] Di Francesco M, Giddings PF, Scott M, Goodman E, Anno GD, Potter K. Influence of laser power density on the meso - structure of thermoplastic composite preforms manufactured by automated fibre placement. Long Beach, US: SAMPE Long Beach; 2016.
[44] Khan MA, Mitschang P, Schledjewski R. Parametric study on processing parameters and resulting part quality through thermoplastic tape placement process. J Compos Mater 2013;47:485–99. http://dx.doi.org/10.1177/0021998312441810.